Slug Battery: An Enzymatic Fuel Cell Tested *in vitro* in *Aplysia californica* Hemolymph

Theo Cockrell[1], Kevin Dai[2], Michael J. Bennington[2], and Victoria A. Webster-Wood[2,3(✉)]

[1] Department of Electrical and Computer Engineering, Carnegie Mellon University, Pittsburgh, PA, USA
[2] Department of Mechanical Engineering, Carnegie Mellon University, Pittsburgh, PA, USA
vwebster@andrew.cmu.edu
[3] McGowan Institute for Regenerative Medicine, Carnegie Mellon University, Pittsburgh, PA, USA

Abstract. Supplying continuous power is a major challenge in the creation and deployment of sensors and small robots for marine applications. Glucose-based enzymatic fuel cells (EFCs) are a possible solution for sustainably powering such devices when mounted on or implanted in living organisms. The two main barriers to developing implantable EFCs for marine organisms are their power output and *in vivo* feasibility. Ideally, an *in vivo* EFC should be minimally invasive, remain mechanically secure, and output relatively consistent power over a predefined lifespan, ranging from weeks to months. The shape and chemistry of EFC electrodes can each contribute to or detract from the overall power production potential of the cells. This paper assesses the feasibility of EFCs using the marine sea slug, *Aplysia californica*'s, hemolymph as an analyte and presents methods to enhance the power produced by EFCs by altering their chemistry and form factor. We found that perfluorodecalin-soaked cathodes and spirally-rolled cells demonstrated increased power output compared to their respective control specimens. Cells tested in *Aplysia* saline mirrored the power output trends of cells tested in hemolymph but with higher power output. This work suggests the feasibility of creating implantable EFCs for marine sea slugs that could one day serve as sustainable biohybrid robotic platforms.

Keywords: Enzymatic Fuel Cell · *Aplysia* · Hemolymph

This work was supported by NSF DBI2015317 as part of the NSF/CIHR/DFG/FRQ/UKRI-MRC Next Generation Networks for Neuroscience Program, by the NSF Research Fellowship Program under Grant No. DGE1745016, and by internal funding through Carnegie Mellon University. Any opinions, findings, and conclusions or recommendations expressed in this material are those of the authors and do not necessarily reflect the views of the National Science Foundation.
T. Cockrell and K. Dai—These authors contributed equally to the work.

F. Meder et al. (Eds.): Living Machines 2023, LNAI 14158, pp. 318–334, 2023.
https://doi.org/10.1007/978-3-031-39504-8_22

1 Introduction

As commercial electronic devices have become smaller and more energy efficient, it has become feasible to create small-scale electronic devices and sensors for wearable and implantable applications [14]. However, powering these devices for long-term usage typically requires long charging cycles or may otherwise result in limited lifetimes [1]. Powering electronic payloads for long-term environmental monitoring poses unique challenges. Devices may need to be deployed for long periods in various environmental conditions without human intervention [6] and with limited access to charging infrastructure.

In marine environments, powering these devices is further hindered by reduced access to sunlight and harsh salinity conditions. Despite these limitations, marine environments may be among the most compelling application spaces for low-power, sustainable power sources due to the need for persistent aquatic sensors that monitor ongoing changes in ocean ecosystems. For these same reasons, sustainably-powered sensors could be utilized in the rapidly growing field of aquaculture [6,13]. Su et al. detailed the many factors that affect water quality and aquaculture cultivations [13]; some of these factors, including pH, temperature, and salinity, are able to be measured by sensors with power requirements in the microwatt range [12].

One possible solution to sustainably power implantable sensors and microelectronics is an enzymatic fuel cell (EFC) that consumes glucose [6,14]. Glucose-based EFCs generate electricity through biocatalytic oxidation of glucose at the anode [5]. A number of implantable biofuel cells have been previously reported in the literature, including in the retroperitoneal space of rats [2], in rabbit blood vessels [3], in the caudal area of fish [6], in the hemocoel of lobsters [10], and in living land snails [5]. However, to our knowledge, no biocatalytic EFCs have been previously developed for use in sea slugs to target marine applications.

To begin addressing the need for implantable fuel cells in marine applications, we have developed enzymatic fuel cells for use with hemolymph from the marine sea slug, *Aplysia californica*. *Aplysia*'s body structure lends itself to the introduction of glucose-based EFCs due to its large body cavity and open circulatory system [9]. In this work, we build on the state-of-the-art in implantable EFCs and compare the performance of EFC designs in *Aplysia* hemolymph. Through a series of benchtop proof-of-concept studies, we have identified the baseline performance of these cells and demonstrated the effect of perfluorodecalin treatment on cell voltage in hemolymph. These preliminary studies suggest the feasibility of using enzymatic fuel cells to power future implantable aquatic sensors in *Aplysia* for applications including marine environmental monitoring.

2 Methodology

Two battery geometries, two electrode chemistries, and two testing solutions were evaluated in a fractional design of experiments to establish feasibility and identify process improvements for an *Aplysia* hemolymph-powered enzymatic

fuel cell (EFC). The electrodes utilized a chemical reaction that converted glucose and oxygen to electricity and water, building on prior work demonstrated in land snails [5]. In addition to testing the electrode chemistry described by Halamkova et al., we compared the performance of cells with and without the addition of perfluorodecalin to the cathode [5]. Perfluorodecalin is a fluorocarbon that acts as a solvent for oxygen, allowing higher oxygen concentrations to be dissolved in the working fluid [7]. We hypothesized that perfluorodecalin's oxygen-transporting properties could increase local oxygen concentration at the cathode, and thus increase power output [8]. We also compared the performance of a rolled cell, with cathodic perfluorodecalin, in both extracted hemolymph and *Aplysia* saline. We decided to use *Aplysia* saline for our tests since previous works had proved it to be an appropriate analog for sea slug hemolymph [11]. Other works had also used an analog solution to mimic the properties of hemolymph in their earlier testing [5]. By using *Aplysia* saline in all experiments that did not depend on hemolymph itself as a variable, we only had to extract hemolymph from *Aplysia* one time. This minimized the harm done to the animal since hemolymph extraction could be detrimental to the slug, especially if multiple extractions are performed.

2.1 Electrode Fabrication

All electrodes used in this work were built using a multi-wall carbon nanotube (MWCNT) base material (20 gsm buckypaper, Nano Tech Labs), adapting procedures described by Halamkova et al. [5]. Briefly, to prepare the electrodes, MWCNT strips were manually cut from the stock material using a razor blade to a size of 52.6 mm × 14 mm (Figure 1). All electrode strips underwent a three-step wash preparation with gentle shaking at 60 RPM via an orbital shaker (VWR 3500I) at 21°C. First, electrodes were submerged in 10 mM 1-pyrenebutanoic acid succinimidyl ester (PBSE, VWR) in dimethyl sulfoxide (DMSO, Thermo Fisher Scientific) for 1 h. Electrodes were then transferred to DMSO and washed for 5 min. Finally, electrodes were transferred to a 10 mM potassium phosphate buffer for an additional 5 min.

Following the three-step wash process, the anode and cathode materials underwent separate preparation steps. All anodes were incubated in 1 mg/mL PQQ-dependent glucose dehydrogenase (PQQ-GDH, Toyobo) and 1 mM $CaCl_2$ in potassium phosphate buffer (10 mM, pH 7) for 1 h with gentle shaking. In contrast, cathodes were incubated in 1.5 mg/mL laccase from *Trametes versicolor* (Sigma-Aldrich) in 10 mM potassium phosphate buffer (pH 7) for 1 h with gentle shaking. For cells constructed with perfluorodecalin, the cathode was then shaken in 0.1 M perfluorodecalin in de-ionized water for an additional hour. EFCs constructed without the addition of perfluorodecalin were considered "control chemistry" cells for our data analysis. Anodes and non-perfluorodecalin cathodes were stored in separate containers containing 0.1 M potassium phosphate buffer until they were tested or used to create a cell. Cathodes that were soaked in 0.1 M perfluorodecalin were kept in the perfluorodecalin solution at 4°C until testing or construction.

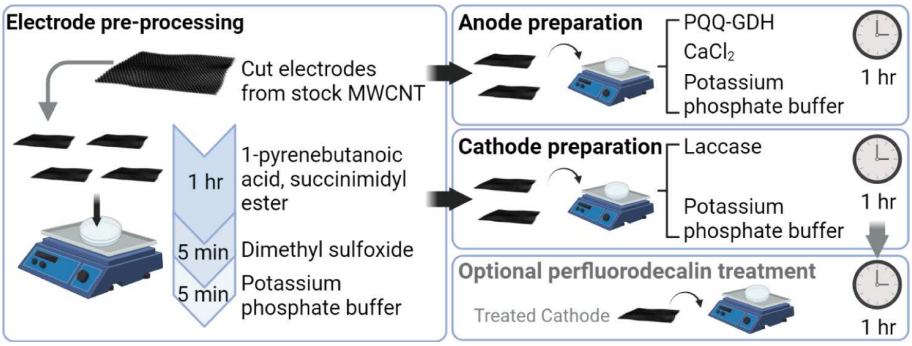

Fig. 1. Electrode fabrication process for glucose-based enzymatic fuel cells. The electrodes are fabricated from buckypaper with multi-wall carbon nanotubes and soaked in a series of solutions that will coat the electrodes in their respective enzymes. All electrodes follow the same series of pre-processing solutions. Then, the anodes are incubated with PQQ-dependent glucose dehydrogenase and the cathodes are incubated with laccase. Some cathodes are additionally coated with perfluorodecalin for improved oxygen transport.

2.2 Elastomer Separator Fabrication

The two EFC electrodes should be separated by a thin gap that prevents shorting and reduces the cell's internal resistance, while simultaneously providing sufficient fluid flow between the electrodes for fresh reagent to contact the electrodes' surfaces. To create this gap, a hollow-frame elastomeric separator was designed with 0.3 mm-thick walls on the upper and lower surfaces and a 0.5 mm-thick gap between walls (Fig. 2). 4.5 mm × 5 mm cutouts in the walls enable fluid to contact the electrodes and are supported by 2.4 mm × 12.2 mm pillars between the walls. The separator was constructed out of a flexible elastomer (Asiga DentaGUM, Shore 30A) on an Asiga Pico 2 HD printer (27 µm XY resolution, 0.1 mm layer height) to enable rolling the electrodes into cylindrical cell geometries. The length and width of the separator measured 50.8 mm × 14 mm. The length of the separator was undersized compared to the electrodes to provide potential capability for wrapping the electrodes around their respective wires for better electrical contact, although the wrapping was not implemented in the work presented here.

2.3 Enzymatic Fuel Cell Construction

Each cell was constructed using one anode and one cathode, three 3D-printed elastomer separators, and two wires (Fig. 3). Cyanoacrylate adhesive (CA 100, Mitreapel) was used to attach all layers at their centers and edges.

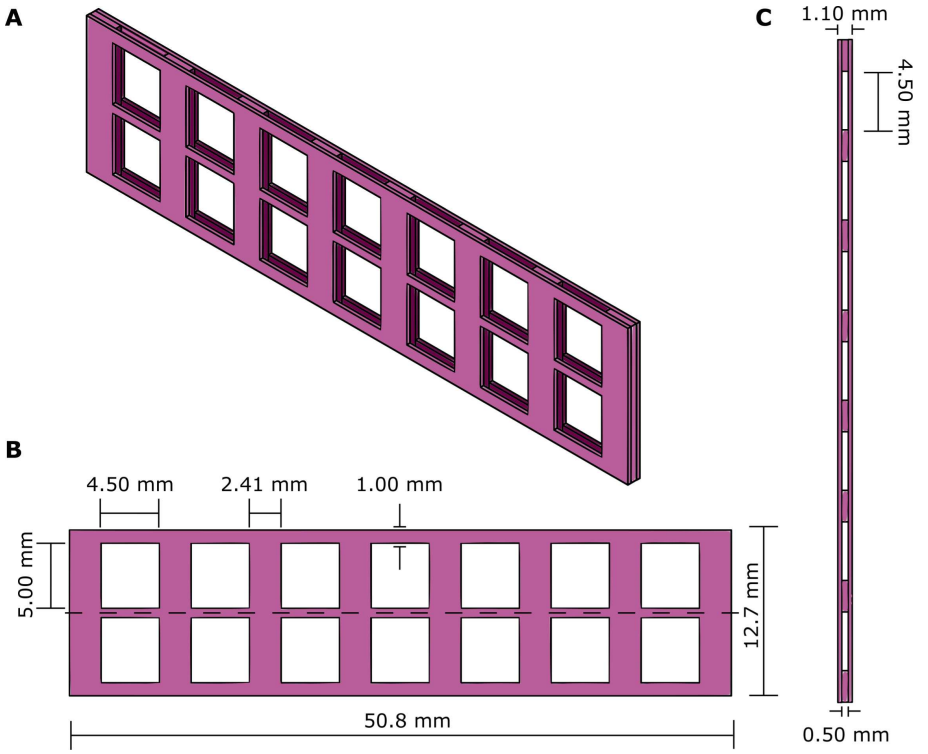

Fig. 2. a) Isometric view of a hollow elastomer separator, 3D printed from Asiga DentaGUM, which separates the electrodes of the battery while enabling fluid flow between the electrodes. b) Front view of a separator. c) Top view of a separator. Due to the flexibility of the elastomer, both flat and rolled cell geometries can be constructed using the same separator design.

"Flat" Cell Construction. A flat enzymatic fuel cell design was created by sequentially layering the electrodes between elastomer separators, with conductive wire (24 AWG) sandwiched between each electrode and their respective outer elastomer separator. The electrodes were attached to the separators using cyanoacrylate adhesive at their centers and their edges. The wires were attached to the electrodes by applying cyanoacrylate adhesive to a 3 mm section of the 12 mm-long bare wire contacting the electrode, while leaving the remainder of the bare wire free of adhesive.

"Rolled" Cell Construction. A rolled cell geometry, inspired by the power-dense jelly-roll design of electrolytic capacitors, was also designed and tested. The spiral winding of the rolled cell was hypothesized to facilitate more chemical reactions and decrease electrical resistance between the two electrodes due to an increased active surface area; by rolling the cell, each side of the cathode

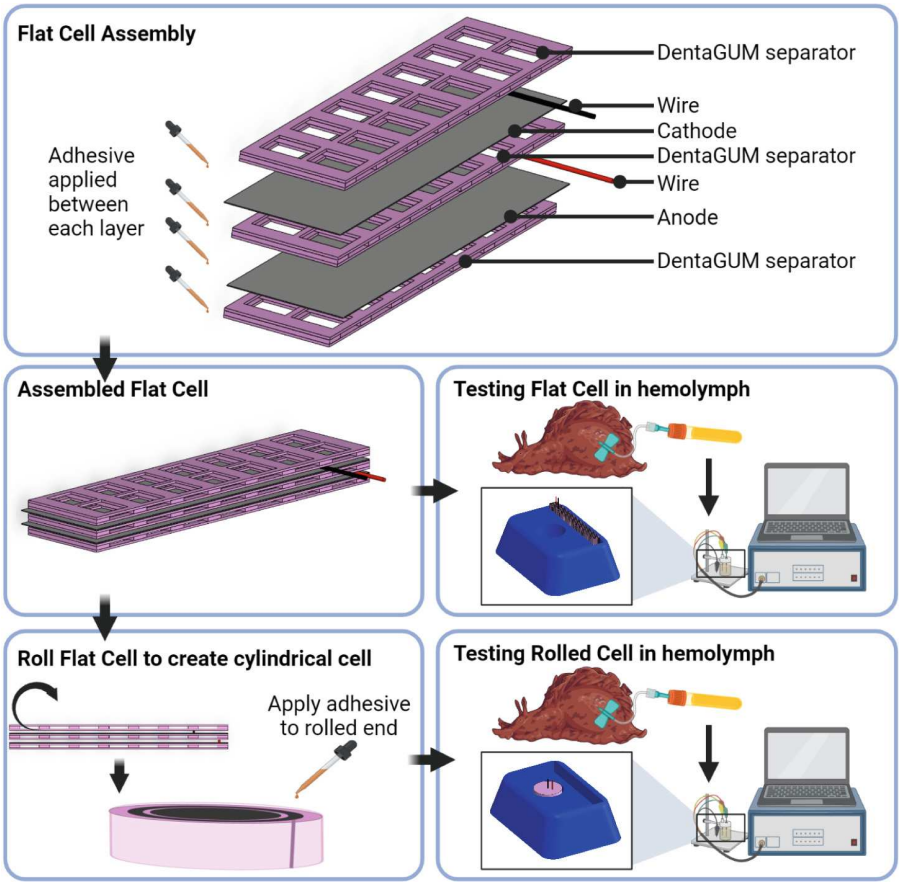

Fig. 3. The tested EFCs are assembled by layering electrodes between thin elastomer separators (DentaGUM). Each EFC uses two electrodes, three elastomer separators, and two conductive wires. Wires are stripped bare and placed adjacent to their respective electrode before sandwiching between elastomer separators. Cyanoacrylate adhesive secures the assembled cells together. Rolled cells are formed by rolling a completed flat cell along its length. Assembled cells are placed in a 3D-printed test stand (blue), which contains wells for either cell form factor. Extracted *Aplysia* (Color figure online) hemolymph or synthetic *Aplysia* saline is applied to the cell during testing. In each test, the load resistance across the cell is varied by a microcontroller and the cell voltage is continuously logged to a PC.

would face the anode, and vice versa. To create a rolled cell, we first created a complete flat cell and then rolled the cell length-wise. To ensure that the cylindrical structure was maintained, cyanoacrylate adhesive was applied to attach the loose end of the cell to the rest of the body.

2.4 Testing

The performance of each EFC geometry was tested in *Aplysia* saline and hemolymph using electrodes constructed with and without perfluorodecalin. We designed a polyethylene terephthalate (PETG) 3D printed benchtop test stand (Fig. 3) containing a well to hold a flat EFC and a well to hold a rolled EFC, which was used for all tests. Flat and rolled EFCs could be fully submerged in 6 mL and 4 mL of hemolymph, respectively, minimizing the amount of hemolymph that needed to be extracted from the animal for testing. For flat cells, the rectangular hemolymph well measured 55 mm × 7 mm × 15 mm. For round cells, the cylindrical well measured 9 mm radially and 15 mm deep.

All experimental data were collected using a Teensy 4.0 microcontroller's onboard 10-bit analog-to-digital converter (ADC) to read the analog voltage output of the EFC. Analog voltage data was logged at a 1 kHz sampling frequency and saved to a text file on a PC through serial communication (PuTTY, 9600 Hz baud rate) from the Teensy microcontroller. A varying resistive load was placed across the cell by combining fixed-value resistors ($R_f \in [0\Omega, 4.7\ \text{k}\Omega, 10\ \text{k}\Omega, 22\ \text{k}\Omega, 47\ \text{k}\Omega]$) in series with a variable load resistance (667–4000Ω range). The variable load resistance was constructed from three 10 kΩ digital potentiometers (Adafruit DS3502, 7-bit or 128 levels) in parallel. We noted that the individual digital potentiometers had an average wiper resistance of 2 kΩ when 15 V was applied to the V_+ terminal, which is why the minimum variable load resistance was 667Ω even with all three parallel potentiometers set to their minimum potentiometer resistance of 0Ω. We used an LCR meter (Atrix MCR-5030) to verify that the variable load resistance was within 10Ω of the expected 4000Ω resistance value when all three potentiometers were set to their maximum potentiometer resistance of 10 kΩ.

For each experimental configuration that was tested (Table 1), EFCs were submerged in either hemolymph or *Aplysia* saline, and the voltage was recorded during a sweep of resistance values, beginning at $(667 + R_f)\Omega$ and ending at $(4000 + R_f)\Omega$, where R_f is the resistance of the fixed-value resistor. To provide the varying load resistance, only one of the three potentiometers was actively changed at a time while the other two inactive potentiometers were held at either 0Ω or 10 kΩ, depending on whether or not they had been previously active. The actively changing potentiometer was monotonically swept from 0-10 kΩ in single level steps corresponding to a 78Ω step increase in potentiometer resistance. The EFC's analog voltage was sampled 50 times at the 1 kHz sampling frequency for each step change in resistance. With a 6 ms pause before transitioning to the subsequent resistance values, each resistance value was set for a total time of 56 ms. Since the variable load was swept through 384 resistance values, one full sweep of load resistances spanned 21.5 s. Once the actively changing potentiometer reached a resistance of 10 kΩ, it was held at a static resistance of 10 kΩ while the next potentiometer was swept from 0-10 kΩ. When all three potentiometers had completed their sweeps and were each held at resistances of 10 kΩ (+2 kΩ of wiper resistance), the EFC's load resistance had reached its final value of $(4000 + R_f)\Omega$. Considering the 2 kΩ wiper resistances and

Table 1. Experimental conditions and parameters. *Italics* indicate the independent variable for a particular test type.

Test Type	EFC Specimen	Experimental Variables		
		Form Factor	Perfluoro. (Y/N)	Testing Fluid
Cell Form Factor	1	*Rolled*	N	Hemolymph
	2	*Flat*	N	Hemolymph
Perfluorodecalin v. Control Chemistry	1	Rolled	*N*	Hemolymph
	2	Flat	*N*	Hemolymph
	3	Rolled	*Y*	Hemolymph
	4	Flat	*Y*	Hemolymph
Testing Fluid	3	Rolled	Y	*Hemolymph*
	3	Rolled	Y	*Saline*

the parallel arrangement of the three potentiometers, each 78Ω step increase in potentiometer resistance corresponded to a change in EFC load resistance that varied between 0.5-43.9Ω, depending on the resistances of the static potentiometers.

2.5 Hemolymph Extraction

A wild-caught *Aplysia californica* specimen (421 g) was obtained from Marinus Scientific (Long Beach, CA) and maintained in a 40 L tank of artificial sea water (16°C, specific gravity 1.026). Hemolymph was extracted from this animal in a survival procedure using the anesthetization protocol described by Gill et al. (2020) [4]. Briefly, the animal was anesthetized with a 30% (volume [mL]: body mass [g]) injection of 333 mM magnesium chloride. The injected fluid was spread throughout the body with manual palpation. Then the animal was transferred to a bath of 2–5°C artificial seawater and allowed to chill for 10 min. Approximately 20 mL of hemolymph was then drawn from the animal with a syringe. For both the injection and extraction, 21 gauge needles were used, and all punctures were sealed with cyanoacrylate adhesive (Mitreapel). To avoid vital organs, the injection and extraction points were placed in the cheek of the animal, below the buccal mass. The extracted hemolymph was stored in a 100 mL specimen jar for testing immediately after the surgery. After testing, the extracted hemolymph container was stored at 4°C. *Aplysia* saline was created following the process outlined by McManus et al. [11] and also stored at 4°C.

3 Results

3.1 "Flat" Vs. "Rolled" Cells

Rolled cells demonstrated a much higher peak power compared to flat cells (Fig. 4). For flat cells, the mean and standard deviation of peak power was

0.83 ± 0.04 μW at 5390Ω. For the rolled cell, the power spiked to 6.94 ± 0.41 μW and 7.29 ± 0.16 μW at 667Ω and 5370Ω, respectively. Above resistances of 5370Ω, the power output of both cells decreased with increasing resistance.

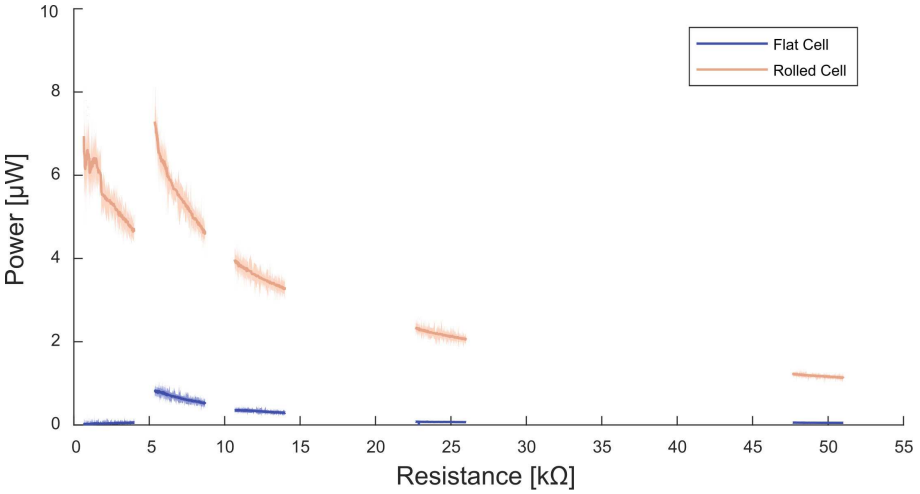

Fig. 4. Both flat and rolled cell geometries were tested in *Aplysia* hemolymph using 52.6 mm long electrodes that were not coated in perfluorodecalin. The rolled cell exhibits a much higher power output than the flat cell, especially at load resistances lower than 10.7 kΩ. The power from both cells decreases with increasing resistance after 5370Ω. The rolled cell shows two peaks in power, which is not expected because cells typically exhibit a single power peak. This double power peak could be due to charge that built up in the EFC prior to testing and dissipated once the cell was put under a load, or due to rapid consumption of reagents at low load resistances. Solid lines show the mean power value for a given resistance, with shaded regions showing the full range of measured power values.

3.2 Cells with Perfluorodecalin Vs. Without

The addition of perfluorodecalin to the electrode chemistry of a rolled cell led to an increase in power output (Fig. 5A). At their respective peaks, the control chemistry cell output 7.29 ± 0.16 μW while the cell with perfluorodecalin output 15.1 ± 0.34 μW, a 107% increase in power. For the cell without perfluorodecalin, we note two peaks at 667Ω and 5370Ω, whereas the peak power for the cell with perfluorodecalin is measured at 1500Ω. Both cells exhibit a visually similar trend in slope at resistances above 5370Ω.

In contrast to the rolled cell, a flat cell that utilized perfluorodecalin was not consistently more powerful than a flat cell utilizing the control chemistry (Fig. 5B). The cell with control chemistry produced a peak power of 0.83 ± 0.04 μW at 5390Ω, which was 207% greater than the peak of 0.27 ± 0.03 μW

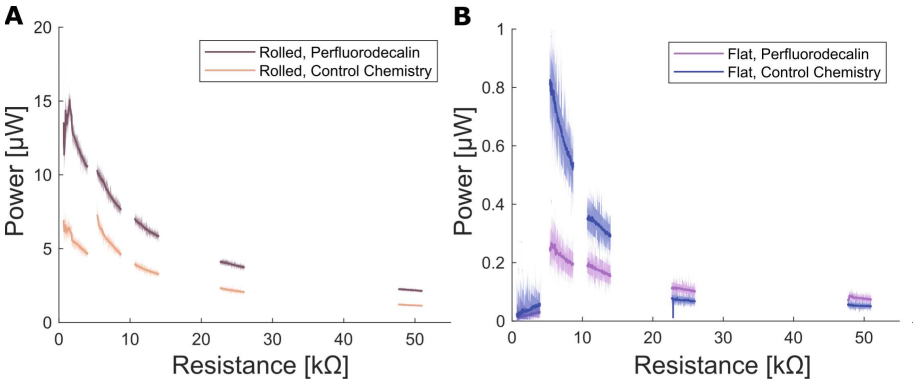

Fig. 5. Power comparisons of (A) rolled and (B) flat cells in hemolymph with different electrode preparations. (A) Using perfluorodecalin with rolled cells led to a 100% peak power increase compared to control chemistry. Both cells demonstrate visually similar slopes at resistances above 5370Ω. (B) For flat cells, the control chemistry cell demonstrated a peak power of 0.83 ± 0.04 μW, which was 207% higher than the peak power produced by the cell with perfluorodecalin, 0.27 ± 0.03 μW. This was substantially less than the power levels observed in the rolled cells. The power from both cells decreases with increasing resistance after 5370Ω. As before, solid lines show the mean power level for a given resistance, with shaded regions showing the full range of measured powers. In this preliminary study, it is unclear why the flat and rolled cells showed opposite effects of the perfluorodecalin treatment, but this should be further investigated in future work.

produced by the cell with perfluorodecalin at 5620Ω. It was only at resistances above 22.7 kΩ that the cell with perfluorodecalin began to produce more power than the control chemistry cell consistently.

3.3 Submerged in *Aplysia* saline vs. Submerged in Extracted Hemolymph

The rolled cell with perfluorodecalin demonstrated visually similar trends when submerged in either *Aplysia* saline or extracted *Aplysia* hemolymph, albeit with a higher power output in *Aplysia* saline (Fig. 6). Tests in *Aplysia* saline yielded a 70% peak power increase compared to the peak power from tests in hemolymph. In both tested fluids, the rolled cell exhibited visually similar slopes at resistances above 5370Ω. The *Aplysia* saline data set demonstrated a double power peak at 683Ω and 1470Ω, measuring 25.7 ± 0.74 μW and 25.1 ± 0.46 μW respectively. The hemolymph data set exhibited a single 15.1 ± 0.34 μW power peak at 1500Ω.

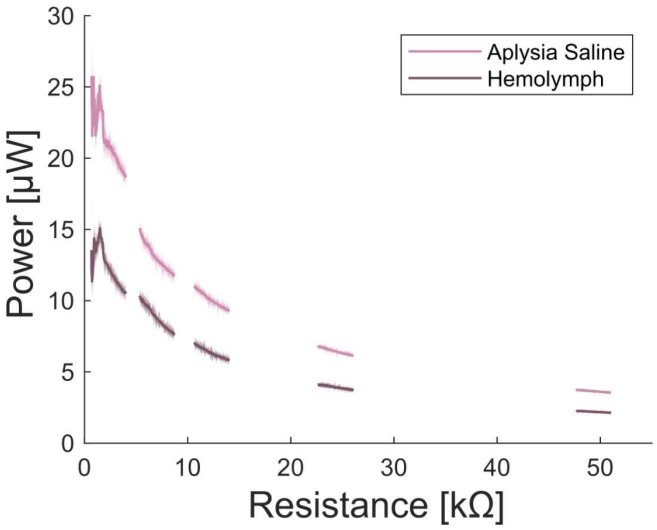

Fig. 6. The perfluorodecalin-treated rolled cell demonstrated visually similar trends in both *Aplysia* saline and hemolymph, but generated a 70% higher peak power output when submerged in *Aplysia* saline. As before, solid lines show the mean power level for a given resistance, with shaded regions showing the full range of measured powers.

4 Discussion

4.1 Analysis of Results

We observed that variables such as changing to a rolled cell geometry and adding perfluorodecalin each impacted the peak power output of our EFCs more percentage-wise than changing the testing fluid. Given the identical fabrication methods between flat cells and rolled cells prior to rolling, we expected a slight increase in power due to a more secure connection between the wires and electrodes in the rolled cell. Instead, even with the control chemistry, we saw an increase in peak power for rolled cells vs. flat when testing in hemolymph. Note that in the tests with rolled cells, the power output was in the 1.13 μW to 7.29 μW range, while the tests with flat cells were consistently lower in the 0.01 μW to 0.83 μW range. This could be due to the spiral winding of the rolled cell, which may create better contact between the wires and electrodes of the rolled cell when compared to the flat cell. We noticed that the cells' power outputs were sensitive to small perturbations in the wire, so we attempted to keep the wires stable during testing. However, the contact between the wire and the cells' electrodes could vary regardless of whether the wires were held manually or mounted on an external fixture. We also note that the choice of alligator clips and method of clamping to the EFC wires may have had an effect on the observed difference in power output of rolled and flat cells. Alligator clips were used to connect to the rolled cells, while mini probe hooks were used to

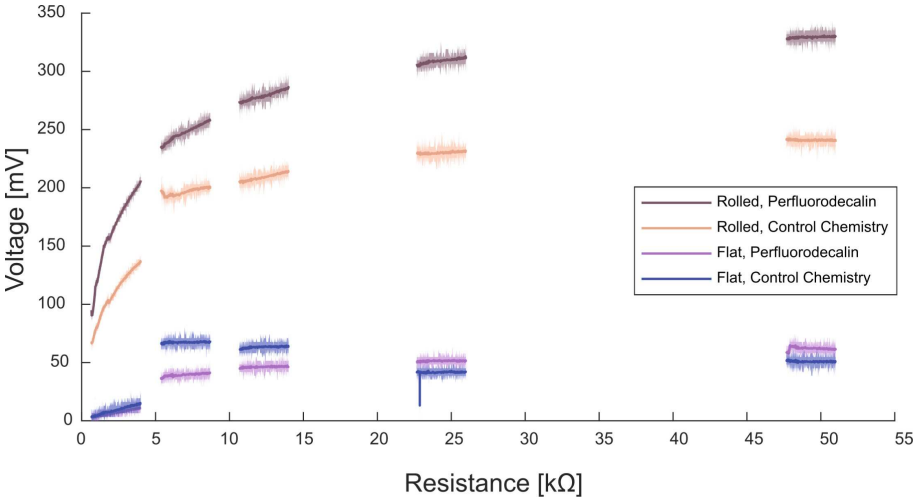

Fig. 7. Across multiple EFC specimens of different compositions, the cell voltage appears to plateau with increased load resistance. The inverse relationship between power and resistance, demonstrated by all tested cells, is due to the plateau in voltage at higher resistances. EFCs with higher peak power output also had higher voltage. Similar to earlier plots, lines show the mean voltage level for a given resistance, with the shaded region showing the full range of measured voltages.

connect to the wires on flat cells. This was due to varying amounts of exposed wire extending from the cells after fabrication. Mini probe hooks were used for shorter lengths of exposed wire extending from the flat cells compared to the rolled cells. Additional experiments with consistent wire connection methods should be conducted in the future to clarify the difference between rolled and flat cell power output. In the future, application of a conductive adhesive at the wire-electrode connection could improve the performance of any cells suffering from insufficient wire contact. Regardless, rolled cells demonstrated the ability to generate several microwatts across a range of resistances (Fig. 4).

Across all measured resistances, the rolled cell with perfluorodecalin exhibited a power output that was always at least 0.98 μW greater than the rolled cell without perfluorodecalin. The increased power output from cells with perfluorodecalin is expected from previous work [8] that demonstrated increased current density and power output after modifying a cathode with perfluorodecalin. Perfluorodecalin's oxygen-transporting properties can provide greater oxygen concentration at the cathode [8]. As the addition of perfluorodecalin increased our EFC's power output, this implies that oxygen could be the limiting factor in the enzymatic reaction taking place in the cell.

Interestingly, the flat control chemistry cell performed better than the flat cell with perfluorodecalin at resistances below 22.7 kΩ. The perfluorodecalin cell's peak power was only 32% of the peak power generated by the control chemistry cell. While the low power output of the perfluorodecalin cell could be due to

poor wire contact, additional testing with more specimens should be conducted to confirm the results. The implementation of previously suggested methods to improve wire contact, such as conductive adhesive or improved clamping, could help resolve this disparity.

Tests using *Aplysia* saline exhibited higher power output than when using hemolymph with the same rolled cell, which implies that the composition of the testing fluid had an effect on power generation. This could be due to many factors, including fluid conductivity, temperature, or glucose concentration. Increasing temperature or glucose concentration could increase power if the limiting factor was related to enzymatic reaction at the electrodes. Further testing to determine these qualities of the extracted hemolymph and prepared saline could potentially shine a light on the differentiating variable. As the power output curves of cells were visually similar between both solutions with a vertical offset, *Aplysia* saline could potentially be used in the future for benchmark *in vitro* testing of EFCs prior to implantation *in vivo*.

In all of our tests, the output power tended to decrease with increasing resistance, although the trend was sometimes broken at resistances lower than 10.7 kΩ. The relationship between power and resistance can be described by $P = \frac{V^2}{R}$, where P is power, V is voltage, and R is resistance. In tested EFCs, the voltage plateaued at higher resistance values (Fig. 7). As the resistance increased while the EFC voltage stayed near constant, we expected to see decreased power output. However, we also note that our testing methodology could contribute to the inverse relationship between power and resistance. As the EFC's load resistances were sequentially swept from low to high values, reagent depletion could account for reduced power output at higher resistance values in later stages of testing. That being said, each sweep of load resistance between $(667 + R_f)\Omega$ to $(4000 + R_f)\Omega$ was conducted within a span of approximately 20 s for a given value of R_f.

For regions where the cell power increased with increasing resistance, it is implied that the voltage increases sufficiently rapidly to compensate for the inverse relationship with resistance. A special case in our test data occurred when a double power peak was exhibited at resistances below 10.7 kΩ. These double peaks are likely a consequence of previously mentioned issues, such as poor electrical wire contact or limited reagent, but additional testing is needed to confirm. Since these peaks occurred at low load resistances that were the first to be tested in each of our experiments, it is also possible that charge had accumulated on the EFC's electrodes prior to testing and dissipated during experimentation. This charge buildup could be due to the cell's exposure to reagents prior to testing, such as after placing the cell in test solution. Additional testing with alternative experimental methods, such as randomizing the sequence of tested load resistances, could determine if charge buildup is a significant variable.

We note that the method for sweeping the potentiometers' resistance values was not ideal for collecting data at evenly-spaced load resistance values. As mentioned previously, only one potentiometer at a time was actively swept from 0-10 kΩ while the remaining two potentiometers were fixed at values of either 0Ω

or 10 kΩ. This resulted in step changes in load resistance that varied between 0.5-43.9Ω. The smallest, 0.5Ω, step changes in load resistance occurred when the first active potentiometer was sweeping to high potentiometer resistances near 10 kΩ and the remaining inactive potentiometers were held at 0Ω. The largest, 43.9Ω, step changes in load resistance occurred when the third active potentiometer was sweeping from low potentiometer resistances near 0Ω and the remaining inactive potentiometers were held at 10 kΩ. We intend to implement an improved potentiometer resistance sweeping method in future work for more evenly-spaced load resistance values. The improved method would alternate between active potentiometers after each 78Ω step change in potentiometer resistance, such that the difference between any two given potentiometers' resistances is never greater than $2 \times 78\Omega = 156\Omega$. With the improved method for sweep potentiometer resistances, the step change in EFC load resistance will vary between 8.5-9.0Ω, which is a much smaller range than the 0.5-43.9Ω variation exhibited by the current method.

It is also possible that glucose levels in a cell's test solution decreased significantly throughout multiple tests. In future experiments, either a glucose monitor or colorimetric glucose assays will be used to measure the glucose levels in the test solution before and after a test. This should help determine how much glucose levels are decreasing during testing. The test solution will also be replaced after every sweep of load resistances, rather than after testing each cell. This should reduce the temporal impact of glucose consumption on subsequent tests' results.

An interesting point of comparison between our EFC and previous works is the power density of said EFCs. In particular, Halamkova et al. generated a maximum power density of 30 μW cm^{-2} with their implanted biofuel cell [5]. Our rolled cell, when implanted in hemolymph, generated a maximum power density of 0.99 μW cm^{-2}. Further testing and characterization of our EFC should help us understand the difference in power density given the similar electrode fabrication methods.

4.2 Experimental Process Improvements

Through the pilot studies presented here, we have identified several process improvements for reliable EFC fabrication. First, the MWCNT electrodes were prone to tearing during handling in the washing and incubation steps. We found that carefully handling the electrodes away from their edges using curved tweezers was effective at reducing tearing occurrences. Furthermore, large sample containers in which the electrodes are less likely to contact the wall should be used during the incubation steps, as electrodes were more likely to tear after sticking to the container wall. We also found that gently shaking the cathode in 0.1 M perfluorodecalin was sufficient to observe noticeably improved power output, as opposed to using a perfluorodecalin slurry spray [8]. We observed that three 52.6 mm electrodes could be gently shaken in the same container with no loss in efficacy.

Our current cell design uses flexible elastomer separators that maintain a thin gap between the electrodes, which prevents shorting while also allowing fluid flow to carry fresh reagents to the electrode surfaces. As an additional benefit, the flexibility of the elastomer allows any flat cell to be rolled into a rolled cell with minor changes in fabrication methods. The rolled geometry could provide increased active electrode surface area for increased power output. Rolled cell geometry could also be a better option for spaces that are length-constrained or where fluid flow is predominantly in an axial direction rather than through a thin-walled duct. Further development of similar structures that enable high flow rate and high roll density could be beneficial for improving the performance of high power density EFCs.

4.3 Future Work

We identified several routes for future improvements related to experimental design to improve our understanding of the power output provided by EFCs for use in *Aplysia* hemolymph. Among these are reducing variability in electrical contact resistance, improving the sequence of applied load resistances, and evaluating the reagent-limited and time-dependent responses of fabricated cells. As only one specimen was evaluated during each test, additional experimentation is needed to collect data and confirm the trends presented in this paper. In addition, we would consider exploring new electrode materials with higher power output and improved structural integrity [3]. As glucose-based EFCs are developed further, we will consider *in vivo* implantation into aquatic invertebrates such as *Aplysia*, which could enable remote monitoring in harsh marine environments using non-invasive microelectronics. EFC-powered sensors mounted on *Aplysia* could record environmental data and autonomously transfer the data to researchers through nearby relay stations without requiring personnel stationed on site. Since the EFCs are self-sustaining as long as the *Aplysia* continues feeding and producing glucose, we would expect the lifespan of the implanted sensor and integrated circuitry to surpass the lifespan of the animal. The suggested remote sensing capability would ideally enable the monitoring of marine habitats with low environmental impact and minor upkeep.

The power output of the presented EFCs could enable the operation of small sensor payloads by utilizing capacitative charge pump circuitry, as demonstrated by Huang et al. [6]. The available supply voltage could also be increased by connecting multiple EFCs in series. In future experiments, the efficacy of EFC's could be benchmarked by long-term, stable power generation for powering energy-efficient sensors [12].

5 Conclusion

The glucose-based enzymatic fuel cells (EFCs) explored in this paper are a step towards tractable implanted electronics within *Aplysia* for operation in aquatic environments. We found visually similar electrical performance between cells

extracted in *Aplysia* hemolymph and synthetic *Aplysia* saline, which could be used in future benchtop experiments for estimating the performance of *in vitro* electrodes before *in vivo* usage. We also demonstrated the effects of several key factors on EFC power output, including electrode chemistry and cell form factor. Improved power output from electrodes using perfluorodecalin and rolled cell geometry suggests that these design elements should be considered in the further development of EFCs. Additional experimentation with more specimens should be conducted to confirm the trends presented in this paper. Future improvements to EFC designs could investigate alternative electrical connection methods for consistently low contact resistance and utilize alternative base materials for electrodes. As EFCs become more powerful, they could support a realm of applications, including robotic operation in locations without existing infrastructure and self-sustaining aquatic sensors in harsh marine environments.

Acknowledgements. Figures 1 and 3 were created with graphical assets from Biorender.com.

References

1. Chen, X., et al.: Stretchable and flexible buckypaper-based lactate biofuel cell for wearable electronics. Adv. Func. Mater. **29**(46), 1905785 (2019)
2. Cinquin, P., et al.: A glucose biofuel cell implanted in rats. PLoS ONE **5**, e10476 (2010)
3. El Ichi-Ribault, S., et al.: Remote wireless control of an enzymatic biofuel cell implanted in a rabbit for 2 months. Electrochim. Acta **269**, 360–366 (2018)
4. Gill, J.P., Chiel, H.J.: Rapid adaptation to changing mechanical load by ordered recruitment of identified motor neurons. Eneuro **7**(3) (2020)
5. Halámková, L., Halámek, J., Bocharova, V., Szczupak, A., Alfonta, L., Katz, E.: Implanted biofuel cell operating in a living snail. J. Am. Chem. Soc. **134**(11), 5040–5043 (2012)
6. Huang, S.H., Chen, W.H., Lin, Y.C.: A self-powered glucose biosensor operated underwater to monitor physiological status of free-swimming fish. Energies **12**(10), 1827 (2019)
7. Jägers, J., Wrobeln, A., Ferenz, K.B.: Perfluorocarbon-based oxygen carriers: from physics to physiology. Pflügers Arch.-Eur. J. Physiol. **473**, 139–150 (2021)
8. Karaskiewicz, M., Biernat, J.F., Rogalski, J., Roberts, K.P., Bilewicz, R.: Fluoroaromatic substituents attached to carbon nanotubes help to increase oxygen concentration on biocathode in biosensors and biofuel cells. Electrochim. Acta **112**, 403–413 (2013)
9. Koester, J., Koch, U.: Neural control of the circulatory system of Aplysia. Experientia **43**, 972–980 (1987)
10. MacVittie, K., et al.: From "cyborg" lobsters to a pacemaker powered by implantable biofuel cells. Energy Environ. Sci. **6**(1), 81–86 (2013)
11. McManus, J.M., Lu, H., Chiel, H.J.: An in vitro preparation for eliciting and recording feeding motor programs with physiological movements in Aplysia Californica. JoVE (J. Visualized Exp.) (70), e4320 (2012)
12. Olatinwo, S.O., Joubert, T.H.: Energy efficient solutions in wireless sensor systems for water quality monitoring: a review. IEEE Sens. J. **19**(5), 1596–1625 (2018)

13. Su, X., Sutarlie, L., Loh, X.J.: Sensors, biosensors, and analytical technologies for aquaculture water quality. Research **2020**, 1–15 (2020)
14. Wang, L., Wu, X., Su, B.Q.W., Song, R., Zhang, J.R., Zhu, J.J.: Enzymatic biofuel cell: opportunities and intrinsic challenges in futuristic applications. Adv. Energy Sustain. Res. **2**(8), 2100031 (2021)